

# 1 Prospects for dendroanatomy in paleoclimatology – a case study on *Picea* 2 *engelmannii* from the Canadian Rockies

3 Kristina Seftigen<sup>1,2\*</sup>, Marina V. Fonti<sup>2,3</sup>, Brian Luckman<sup>4</sup>, Miloš Rydval<sup>5</sup>, Petter Stridbeck<sup>1</sup>, Georg von Arx<sup>2,6</sup>, Rob Wilson<sup>7</sup>, Jesper  
4 Björklund<sup>2</sup>

5 <sup>1</sup>Regional Climate Group, Department of Earth Sciences, University of Gothenburg, Gothenburg, Sweden.

6 <sup>2</sup>Dendrosciences, Swiss Federal Institute for Forest Snow and Landscape Research WSL, Switzerland

7 <sup>3</sup>Institute of Ecology and Geography, Siberian Federal University, Krasnoyarsk, Russian Federation

8 <sup>4</sup>Department of Geography, University of Western Ontario, London, ON, N6A 3K7, Canada

9 <sup>5</sup>Department of Forest Ecology, Faculty of Forestry and Wood Sciences, Czech University of Life Sciences Prague, Prague,  
10 Czech Republic

11 <sup>6</sup>Oeschger Centre for Climate Change Research, University of Bern, Switzerland

12 <sup>7</sup>[University of St Andrews, Queen's Terrace, St Andrews, Fife, KY16 9TS, UK](https://www.st-and.ac.uk/locations/queen-terrace)

13 \*Corresponding author:

14 E-mail address: [kristina.seftigen@gvc.gu.se](mailto:kristina.seftigen@gvc.gu.se)

## 16 **Abstract**

17 The continuous development of new proxies as well as a refinement of existing tools are key  
18 to advances in paleoclimate research and improvements in the accuracy of existing climate  
19 reconstructions. Herein, we build on recent methodological progress in dendroanatomy – the  
20 analyses of wood anatomical parameters in dated tree rings – and introduce the longest (1585  
21 – 2014 CE) dendroanatomical dataset currently developed for North America. We explore the  
22 potential of dendroanatomy of high-elevation Engelmann spruce (*Picea engelmannii*) as a  
23 proxy of past temperatures by measuring anatomical cell dimensions of 15 living trees from  
24 the Columbia Icefield area. X-ray maximum latewood density (MXD) and its blue intensity  
25 counterpart (MXBI) have previously been measured, allowing comparison between the  
26 different parameters. Our findings highlight anatomical MXD and maximum radial cell wall  
27 thickness as the two most promising wood anatomical proxy parameters for past  
28 temperatures, each explaining 46% and 49%, respectively, of detrended instrumental July-  
29 August maximum temperatures over the 1901–1994 period. While both parameters display  
30 comparable climatic imprinting at higher frequencies to X-ray derived MXD, the anatomical  
31 dataset distinguishes itself from its predecessors by providing the most temporally stable  
32 warm-season temperature signal. Further studies, including samples from more diverse age  
33 cohorts and the adaptation of RCS-based standardization, are needed to disentangle the  
34 ontogenetic and climatic components of long-term signals stored in the wood anatomical traits  
35 and to more comprehensively evaluate the potential contribution of this new dataset to  
36 paleoclimate research.

37 **Keywords:** Dendroanatomy, *Picea engelmannii*, Canadian Rockies, tree rings, latewood  
38 density, temperature reconstruction, paleoclimatology

39

## 40 1. Introduction

41 Tree rings form the backbone of high-resolution palaeoclimatology of the Common Era by  
42 providing precisely dated, annually resolved, spatially widespread and easily accessible  
43 archives of climate proxy data. Tree-ring archives make up more than half of all publicly  
44 available temperature proxy records and are greatly influential in multi-proxy hemispheric-  
45 scale temperature reconstructions (PAGES 2k Consortium 2017). They are vital for spatially  
46 explicit mapping of [the Medieval Climate Anomaly, the Little Ice Age, and other](#) important  
47 climate periods (e.g., PAGES 2k Consortium 2013), and the study of temporally distinct  
48 cooling events caused by volcanic eruptions (e.g., Schneider et al. 2015; Stoffel et al. 2015;  
49 Wilson et al. 2016). Moreover, tree-ring based climate reconstructions play a key role in many  
50 of the emerging proxy-model comparison efforts (e.g., Goosse 2017; Luterbacher et al. 2016;  
51 Pages k-PMIP3 group 2015; Phipps et al. 2013; Seftigen et al. 2017).

52

53 The most frequently and successfully used tree-ring parameters for the study of [past](#)  
54 temperature variations at high latitudes and altitudes are ring width and maximum latewood  
55 density or simply maximum density (MXD) (e.g., Esper et al. 2018). While ring width is the  
56 most easily acquired [proxy](#) of year-to-year variations in climate, the parameter often proves  
57 difficult to interpret as it may represent distorted transformations of the underlying climate (e.g.,  
58 Frank et al. 2010; Lücke et al. 2019). In particular, ring width may exhibit amplified low-  
59 frequency signals (von Storch et al. 2004) resulting from lagged growth processes in response  
60 to climate (Esper et al. 2015) or non-climatic processes (Rydval et al. 2015). Consequently,  
61 the presence of prominent decadal variability should not be taken as evidence of  
62 corresponding variability distribution in climate observations, and an overestimation of low-  
63 frequency signals is often observed (e.g., Franke et al. 2013; Seftigen et al. 2017; Wilson et  
64 al. 2016). The MXD parameter, in contrast, generally contains a stronger climate signal with  
65 higher signal-to-noise ratios (e.g., Briffa et al. 2002; Ljungqvist et al. 2020), as well as less  
66 biological persistence (Esper et al. 2015) and age-related signal-muting (Konter et al. 2016),  
67 and is less influenced by stand disturbances (Rydval et al. 2018). However, a number of recent  
68 studies (Björklund et al. 2020; Björklund et al. 2019; Edwards et al. 2022) have proposed the  
69 accuracy of the MXD parameter to be sensitive to measurement resolution. Björklund et al.  
70 (2019) showed that increasingly lower resolution of MXD data could result in an increased  
71 artificial similarity to the climate response of ring width, and thus that several of the issues  
72 facing ring width as a climate proxy may also represent non-negligible constraints on the MXD  
73 parameter.

74

75 To reduce uncertainties, future reconstruction efforts could profit from the development of new  
76 proxy types and parameters for paleoclimatology, as well as new and expanding

77 methodologies. Recently, dendroanatomy – the analysis of wood anatomical traits in dated  
78 tree rings (Fonti et al. 2010; Pacheco et al. 2018) – has become more accessible through  
79 semi-automated approaches to quantify wood cell anatomy (Prendin et al. 2017; von Arx and  
80 Carrer 2014; von Arx et al. 2016). Analysis of anatomical cell dimensions is now possible at  
81 the scale required for high-quality climate reconstruction over centuries to millennia (Björklund  
82 et al. 2020). Unlike ring width, anatomical traits of temperature-limited conifers appear to be  
83 less affected by biological memory effects and are imprinted with strong and mechanistically-  
84 grounded temperature signals (Björklund et al. 2019; Cuny et al. 2019; Cuny et al. 2014).  
85 Moreover, cell anatomical measurements have unprecedentedly high temporal resolution  
86 relying on the base unit of the xylem – the tracheid cell, and their biological foundations and  
87 functional links are comparably well understood (e.g., Bouche et al. 2014; Pittermann et al.  
88 2011; Wilkinson et al. 2015).

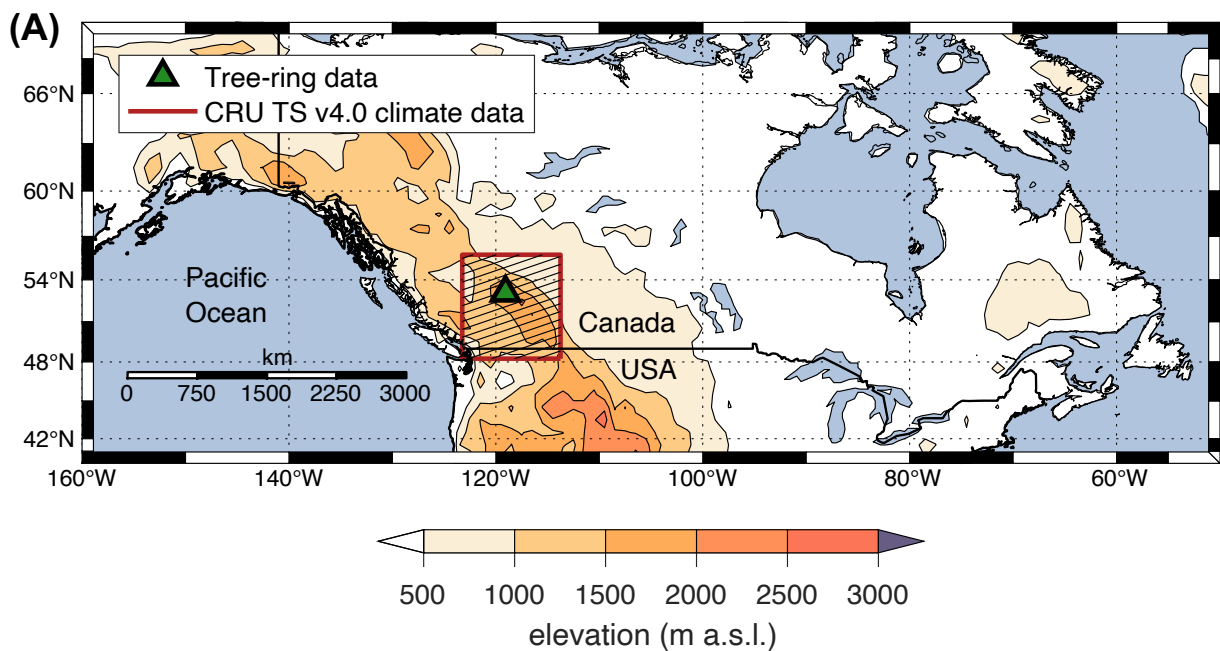
89  
90 In this article, we aim to explore the value of dendroanatomy for high-elevation living  
91 Engelmann spruce (*Picea engelmannii*) trees as a proxy of past temperatures. We make use  
92 of tree samples from the Columbia Icefield area of the Canadian Rockies (Fig. 1) – a site  
93 known for hosting the longest (950–1994 CE) available temperature-sensitive tree-ring  
94 densitometric collections for boreal North America (Luckman et al. 1997; Luckman and Wilson  
95 2005). The Icefield collection, originally comprising ring width and MXD measurements, have  
96 previously been used in regional (Luckman 1997; Luckman 2000; St. George and Luckman  
97 2001) and hemispheric-scale (Briffa et al. 2002; D'Arrigo et al. 2006; Esper et al. 2002; Mann  
98 et al. 1999) temperature reconstructions, including the recent large-scale Northern  
99 Hemisphere summer temperature reconstruction syntheses (Anchukaitis et al. 2017;  
100 Schneider et al. 2015; Wilson et al. 2016). The analysis of the new dendroanatomical dataset  
101 produced here includes an assessment of its signal strength and the imprint of temperature  
102 within a number of wood anatomical traits spanning the period 1585–2014 CE. We detail  
103 common variance amongst selected anatomical parameters and emphasize the  
104 reconstruction potential of this dataset. The availability of MXD from the Columbia Icefield area  
105 (Luckman et al. 1997; Luckman and Wilson 2005), produced with the Walesch Electronic  
106 Dendro2003 technique (Eschbach et al. 1995) and its predecessor (Schweingruber et al.  
107 1978) (hereafter referred to as X-ray MXD), and latewood blue-intensity (referred to as MXBI)  
108 (McCarroll et al. 2002) measurements allow for an optimal opportunity for testing the skill and  
109 potential advantages of dendroanatomical parameters as climate proxies. This work is part of  
110 a larger ongoing collaborative effort dedicated to developing a network of long (~500–1000  
111 years) wood dendroanatomical chronologies across the northern hemisphere. The ultimate  
112 ambition of this initiative is to sharpen signal interpretations of the dendrochronological records

113 and to optimize seasonal and temporal fidelity of the proxy-based reconstructions in order to  
114 revise (or reinforce) previous conclusions about pre-industrial climate variability and the  
115 mechanisms causing this variability. This work also represents a first step towards a  
116 millennium long anatomical *P. engelmannii* dataset for the Columbia Icefield area, Canada.  
117

## 118 2. Data and methods

### 119 2.1 Sample preparation and dendroanatomical measurements

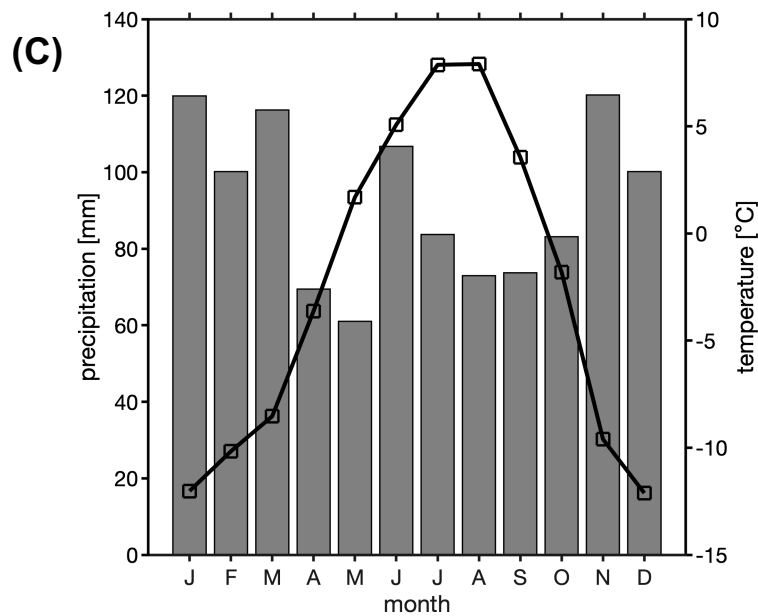
120 Fifteen living *P. engelmannii* trees (one core per tree) were selected for dendroanatomical  
121 measurements from a collection sampled in 2015, from tree-line sites (2000–2100 m a.s.l.)  
122 adjacent to the Athabasca Glacier in the Columbia Icefield area of the Canadian Rockies  
123 (52.13 N, 117.14 W) (fig. 1). The selection of cores was based on 1) the visual appearance of  
124 the material (cores with obvious defects were avoided), 2) the temporal coverage of the series  
125 (we strived to have an even replication through time) and, 3) the common signal strength  
126 based on RBAR statistics (Wigley et al. 1984) of the ring-width measurements (in general,  
127 cores with higher than average RBARs were selected for wood anatomy). The selection was  
128 primarily dictated by 1) and 2), and only secondarily by 3).



129



130



131

132 **Figure 1:** A) Location of the Columbia Icefield site, Canadian Rockies where wood cores for  
 133 dendroanatomical measurements were collected in 2015. B) The tree-ring sampling site at the  
 134 Columbia Icefields. The view is to the north from the Athabasca Glacier forefield, September  
 135 2018. The 2015 samples were obtained from sites east and west of the Icefields Centre  
 136 (building located in the middle of the image). The Athabasca Glacier extended to the foot of  
 137 the slope in the left of the photo in the 1840s. C) Monthly mean temperature and total  
 138 precipitation (1970–2018 averages) for the CRU TS v4.03 grid point (52.25° N, 117.25° W)  
 139 covering the Columbia Icefield area.

140

141 Wood cores were refluxed in alcohol for 24 hours using a Soxhlet apparatus to remove resin  
 142 and other soluble substances, and subsequently embedded in paraffin using a Tissue  
 143 Processor TP1020 and Histocore Arcadia Embedding Center (Leica, Germany). A rotary  
 144 microtome RM2245 (Leica Biosystems, Germany), equipped with N35 disposable microtome  
 145 blades (Feather, Japan), were used to cut 12 μm thick transverse sections from the wood

146 cores. The thin-sections were stained with a 1:1 safranin-astrablue solution and mounted on  
147 slides with Euparal (Carl Roth, Germany), following standard procedures (von Arx et al. 2016).  
148 Digital images from each section were taken with a Zeiss Axio Scan Z1 (Carl Zeiss, Germany)  
149 at a resolution of 2.3 pixels  $\mu\text{m}^{-1}$ . Tree-ring borders and individual tracheid cells were then  
150 semi-automatically identified, and ring width as well as the position and anatomical dimension  
151 of each tracheid cell were measured in the digital images using the image analysis software  
152 ROXAS (v3.1) (von Arx and Carrer 2014). The anatomical parameters included, for instance,  
153 cell lumen area and cell wall thickness (CWT), where the latter was measured in four directions  
154 to obtain the average cell wall thickness, i.e. two radial and two tangential cell walls per  
155 tracheid cell (Prendin et al. 2017). Each tree ring was divided into 20  $\mu\text{m}$  wide bands with a  
156 10  $\mu\text{m}$  overlap, parallel to the ring border (the tangential extension of each band encompasses  
157 ~75–100 tracheids). In order to minimize the influence of outliers, for each anatomical  
158 parameter the values of all cells corresponding to the 75<sup>th</sup> percentile within each 20  $\mu\text{m}$  wide  
159 band were retained for further analysis. That is, from the cells within the radial and tangential  
160 extension of each band, the 75<sup>th</sup> percentile of each cell dimension was calculated, building up  
161 intra-annual measurement profiles of CWT, Lumen area, and other anatomical traits. The  
162 maximum parameters (e.g., Max. radial CWT) thus retain the highest value of the profile for  
163 each year, the minimum parameters retain the lowest value of the profile for each year, and  
164 the earlywood and latewood parameters retain the average value of the profile for the  
165 earlywood and latewood portions of the ring, respectively. The anatomical density was derived  
166 as the ratio of wall area to overall cell area (that is, including both wall and lumen area) in each  
167 20  $\mu\text{m}$  wide band. Mork's index (Denne 1989) was used to separate the earlywood and the  
168 latewood portions of the ring. For further details regarding the dendroanatomical  
169 measurements, see (Björklund et al. 2020).

170

## 171 2.2 Chronology development

172 From the potentially large number of possible dendroanatomical parameters, we narrowed  
173 down subsequent analyses to seven parameters of anatomical dimensions, and three wood  
174 density parameters based on anatomical dimensions, which are directly comparable to X-ray  
175 and blue intensity-based microdensitometric parameters. The parameters are listed in [table 1](#).  
176 For comparative purposes, we also retained X-ray derived measurements of MXD (Luckman  
177 and Wilson 2005), and the previously unpublished latewood blue intensity counterpart (MXBI)  
178 measured on *P. engelmannii* from the Columbia Icefield area. The X-ray MXD was produced  
179 using radiodensitometric techniques (Schweingruber et al. 1978) from 1.2-mm-thick laths, cut  
180 using a twin-blade saw along the tree cores but perpendicular to the fiber direction (see  
181 Luckman and Wilson 2005 for details). For the production of MXBI, the methodology outlined

182 in (Rydval et al. 2014) was adopted. The MXBI measurements were conducted using the  
183 CooRecorder software (ver. 8.1) (<http://www.cybis.se/forfun/dendro/index.htm>).  
184 Corresponding time series of ring-width were also obtained and hereafter referred to as  
185 “original ring-width”, as opposed to “ROXAS ring-width”, which were measured in program  
186 ROXAS on the fifteen cores used for the dendroanatomical measurements. The X-ray MXD  
187 and MXBI datasets were originally developed from living trees and snag material, however, to  
188 ensure consistency for the parameter comparison, we used X-ray MXD, MXBI and original  
189 ring-width measurements from living trees only (X-ray MXD: N = 78 series, MXBI: N = 182,  
190 and original ring width: N = 182, see [table 1](#)). The dendroanatomical analysis was performed  
191 on tree cores for which original ring-width and MXBI measurements were available. Thus, an  
192 additional subset based on the fifteen trees was retained for the latter two parameters to  
193 ensure also a direct comparison with the dendroanatomical chronologies. For the full MXBI  
194 dataset (N = 182), we additionally derived eight partly overlapping percentile chronologies  
195 based on *absolute* ring-width ([fig. S1](#)), to assess whether a similar ring-width dependence as  
196 previously reported by Björklund et al. (2019) from Northern Fennoscandia could also be  
197 detected in the Icefields dataset, i.e. a ring-width related differences of MXBI measurements  
198 taken in narrow versus wide rings. The following ring-width percentile intervals were used: 0  
199 – 30<sup>th</sup>, 10<sup>th</sup> – 40<sup>th</sup>, 20<sup>th</sup> – 50<sup>th</sup>, 30<sup>th</sup> – 60<sup>th</sup>, 40<sup>th</sup> – 70<sup>th</sup>, 50<sup>th</sup> – 80<sup>th</sup>, 60<sup>th</sup> – 90<sup>th</sup>, and 70<sup>th</sup> – 100<sup>th</sup> to  
200 derive the sub-sampled MXBI chronologies. Thus, for example, the 70<sup>th</sup> – 100<sup>th</sup> percentile  
201 chronology is computed from MXBI-values measured in the 30% *widest* rings, while the 0 –  
202 30<sup>th</sup> percentile chronology corresponds to MXBI-values from the 30% of the *narrowest* rings.  
203 Unfortunately, a similar comparative analysis was not possible to conduct for the X-ray based  
204 MXD, as the corresponding ring-width measurements originally developed, were unavailable  
205 to us in the current study.

206

207 Since the analysis was performed on data derived from a cohort of same-aged living trees,  
208 capturing low-frequency variability (i.e. decadal and longer) with RCS-type methods is a  
209 challenge (e.g., Briffa et al. 1992). This is because living-trees-only, share potential climate  
210 signal on lower frequencies even if they are aligned by cambial age (trend-in-signal) (Briffa  
211 and Melvin 2011). Any attempt, even using signal-free approaches, will provide indices, that  
212 likely would have to be revised when implementing the same technique on a large multi-  
213 generational material, and ultimately reflect certainty where there is little. Thus, we primarily  
214 focused here on the year-to-year signals in the tree-ring anatomical parameters. To  
215 emphasize the interannual variations, the individual dendroanatomical series were detrended  
216 in the program MATLAB (version R2021a), by 1) fitting a cubic smoothing spline function with  
217 50% frequency response cutoff at 35 years to the raw tree-ring series (Cook and Peters 1981),  
218 2) subtracting the fitted values from the observed values to obtain detrended series (division

219 was used to standardize the ring-width measurements), and finally 3) averaging the detrended  
220 series by simple arithmetic mean to produce the final parameter-specific chronologies  
221 (hereafter referred to as detrended data). The same detrending procedure was performed on  
222 the MXBI, X-ray derived MXD and original ring-width series, in order to obtain data that are  
223 comparable with the dendroanatomical datasets. All chronologies were truncated to the 1700–  
224 1994 period in the subsequent analyses, to ensure a consistent overlap between datasets as  
225 well as a sample depth ranging between 9 and 15 cores for the anatomical dataset.  
226

### 227 2.3 Statistical methods

228 To evaluate the strength of the between-series common signal and establish the replication  
229 needed to obtain mean chronologies meeting the commonly accepted standard, we used the  
230 RBAR (defined as the mean Pearson’s correlation coefficient between all possible pairs of  
231 individual tree-ring series) (Wigley et al. 1984) and Expressed Population Signal (EPS) (Briffa  
232 et al. 1992) statistics. To assess the degree to which the various parameters co-vary, principal  
233 component analysis (PCA) and pairwise correlations were computed over the 1700–1994  
234 period.

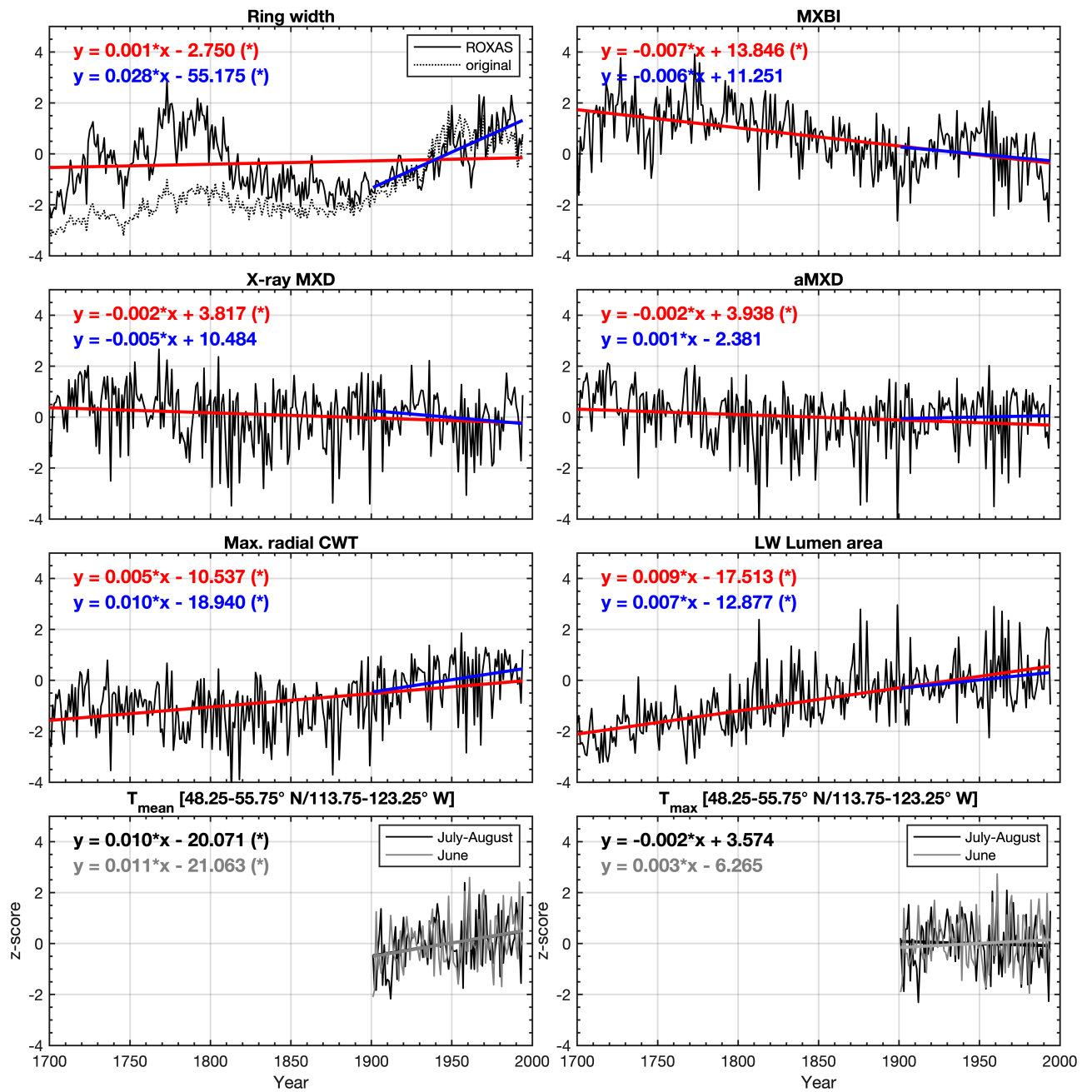
235  
236 Detrended tree-ring parameter chronologies were assessed for their relationship to regional  
237 monthly mean (Tmean) and maximum (Tmax) temperatures, by correlation against the  
238 monthly 0.5° x 0.5° gridded CRU TS v4.03 dataset (Harris et al. 2020) for the grid point  
239 average bounded by the latitude/longitude coordinates 48.25–55.75° N/113.75–123.25° W  
240 (Fig. 1, 2). Tmax was included in the analysis because previous work has demonstrated  
241 slightly stronger calibration statistics than for Tmean when using MXD and ring-width  
242 chronologies for climate reconstruction in this region (e.g., Heeter et al. 2021; Wilson et al.  
243 2019; Wilson et al. 2014; Wilson and Luckman 2003). The associations with monthly  
244 precipitation totals and minimum temperatures were also tested, but not included here due to  
245 weak significant empirical relationships. The lack of precipitation sensitivity of *P. engelmanni*  
246 in the Icefield area was already noted in (St. George and Luckman 2001) which is not  
247 surprising as the trees are growing in temperature limited upper tree-line environments.  
248 Pearson’s correlations were calculated between parameter-specific chronologies and monthly  
249 meteorological variables over the 1901–1994 period, and the 1901–1948 and 1949–1994  
250 subperiod to evaluate temporal stabilities of the climate responses. A paired t-test was used  
251 to test whether the calibration statistics differed between tree-ring parameters and sub-  
252 periods. To make the climate sensitivity analysis comparable to previous studies from the  
253 Columbia Icefield area, we also included the homogenized (1895–present) 50 x 50 km gridded  
254 temperature data (Vincent and Gullett 1999; Zhang et al. 2000) originally developed by the  
255 Meteorological Service of Canada and previously used in Luckman and Wilson (2005) to



256 reconstruct last-millennium summer temperatures for the Canadian Rockies. Similar to  
257 Luckman and Wilson (2005), we used the mean of four grids closest to the Columbia Icefield  
258 area. Calibration trials with these data are provided in the supplement (fig. S2 and S3). To  
259 ensure the climate analysis was not affected by long-term trends, all temperature data were  
260 filtered prior to analysis using the same 35-year filter as was used to detrend the tree-ring  
261 parameters (henceforth referred to as detrended data).

262  
263 Further, the dynamic nature of the temperature signal (i.e. optimal target season and its  
264 temporal stability) was evaluated through moving window correlation analysis between  
265 detrended tree-ring chronologies and detrended daily temperature data (grid 52.5° N, 118.5°  
266 W) from the Berkeley Earth dataset (<http://berkeleyearth.org/data/>) (Rohde and Hausfather  
267 2020) covering the 1880–recent period. Pearson’s correlations were computed for 30-year  
268 sliding windows with a 1-year offset. For each 30-year block, temperatures were averaged in  
269 30-day long windows which were shifted at daily time steps throughout the year (sensu  
270 Jevsenak and Levanic 2018).

271



272

273

274

275

276

277

278

279

280

281

**Figure 2:** Average non-detrended time series of selected tree-ring parameters, z-scored over the 1901–1994 reference period. The blue and red lines show the linear trends over the 1901–1994 and 1700–1994 periods, respectively. Seasonally averaged June–August (48.25–55.75° N/113.75–123.25° W CRU TS v4.03 subset average) mean ( $T_{mean}$ ) and maximum ( $T_{max}$ ) temperatures are provided for comparison. (\*) indicates a significant trend ( $\alpha = 0.05$ ) estimated by the Mann-Kendall trend detection test. Abbreviations used in the figure are LW (latewood), CWT (cell wall thickness), aLWD (anatomical latewood density) and aMXD (anatomical maximum latewood density). See supplement fig. S4 for full 1586–2015 CE period chronologies.

## 282 3. Results and discussion

### 283 3.1 *Picea engelmannii* dendroanatomy characteristics

284 Besides the conventional width parameters (i.e., ring width, earlywood- and latewood width,  
285 referred to as “ROXAS” in [table 1](#)), seven anatomical parameters and three anatomically-  
286 based density parameters were retained for analysis. [Basic chronology assessments of](#)  
287 [detrended data over the common 1700–1994 CE period are provided in table 1, and non-](#)  
288 [detrended mean chronologies for selected parameters are shown in figure 2.](#) In line with  
289 previous [work by Björklund et al. \(2020\) on temperature-sensitive conifers, we find that](#) that  
290 maximum radial cell wall thickness (Max. radial CWT) and anatomical MXD (aMXD) are the  
291 two anatomical parameters with the highest mean inter-series correlation (RBAR = 0.47 and  
292 0.48, respectively). For both parameters, EPS reaches the 0.85 threshold (Wigley et al. 1984)  
293 with 6 series ([table 1](#)). Notably, these values are of comparable strength to the RBAR and  
294 EPS of X-ray based MXD (RBAR = 0.49, 6 trees required for EPS = 0.85). By comparison, the  
295 RBAR for MXBI is surprisingly low at 0.19 and the replication needed to attain the EPS of 0.85  
296 is 24 series. These MXBI chronology statistics are lower than for ring width (RBAR = 0.22 and  
297 0.28 for original and ROXAS ring width, respectively) – an observation noted previously by  
298 (Rydval et al. 2014; Wilson et al. 2019). The RBAR and EPS values for MXBI slightly decrease  
299 if computed only on the 15 trees that have been pre-selected for the dendroanatomical  
300 analysis. This is surprising given that the selection of the cores for dendroanatomy was partly  
301 based on its ring-width signal strength ([see sect. 2.1](#)), and that the RBAR and EPS statistics  
302 for ring width actually improve when narrowing the analyses down to these 15 trees ([see table](#)  
303 [1](#)). Although the BI-based density parameters typically require a larger sample size than ring  
304 width (e.g., Blake et al. 2020; Wilson et al. 2021) for a robust chronology, the MXBI chronology  
305 statistics obtained for *P. engelmannii* from our site are still lower than the previously reported  
306 MXBI findings for the same species across British Columbia, Canada (Wilson et al. 2014).

307  
308 Notably, several anatomical and density parameters are found to exhibit a rather low common  
309 signal, yet a reasonably strong temperature sensitivity ([see sect. 3.2](#)). These include, in  
310 decreasing order of signal strength: earlywood (EW) cell wall area (RBAR = 0.13), EW lumen  
311 area (RBAR = 0.12), EW density (RBAR = 0.10), EW cell area (RBAR = 0.09) and latewood  
312 (LW) cell area (RBAR = 0.09). The replication required to attain robust EPS [statistics](#) ranges  
313 between 38 (EW cell wall area) to 57 trees (EW cell area and LW cell area).

314  
315 **Table I:** Basic summary statistics for each [detrended](#) parameter chronology, [based on the](#)  
316 [common 1700–1994 period](#). Abbreviations used in the table are EW (earlywood), LW  
317 (latewood), CWT (cell wall thickness), aLWD (anatomical latewood density) and aMXD  
318 (anatomical maximum latewood density). [Estimations of the number of trees needed to reach](#)

319 *the arbitrary EPS threshold level of 0.85 are derived from the EPS equation (see Wigley et al.*  
 320 *1984) using the RBAR statistic for each tree-ring parameter. Parameters highlighted in grey*  
 321 *are those requiring the lowest sample replication to reach the threshold level.*

|   | # samples | RBAR                    | n for EPS (0.85)    |
|---|-----------|-------------------------|---------------------|
| <b>Width parameters</b>   |           |                         |                     |
| Original ring-width (from Luckman 1997; Luckman and Wilson 2005, and later unpublished updates) | 182       | 0.22 (0.27 for N = 15)* | 20 (15 for N = 15)* |
| ROXAS ring-width  | 15        | 0.28                    | 15                  |
| ROXAS EW width  | 15        | 0.26                    | 16                  |
| ROXAS LW width  | 15        | 0.19                    | 24                  |
| <b>Earlywood anatomy</b>  |           |                         |                     |
| EW cell area  | 15        | 0.09                    | 57                  |
| EW Lumen area   | 15        | 0.12                    | 42                  |
| EW cell wall area   | 15        | 0.13                    | 38                  |
| <b>Latewood anatomy</b>   |           |                         |                     |
| LW cell area  | 15        | 0.09                    | 57                  |
| LW Lumen area   | 15        | 0.31                    | 13                  |
| Max. radial CWT   | 15        | 0.47                    | 6                   |
| Max. tangential CWT   | 15        | 0.34                    | 11                  |
| <b>Density parameters</b>   |           |                         |                     |
| EW density  | 15        | 0.10                    | 51                  |
| aLWD  | 15        | 0.28                    | 15                  |
| aMXD  | 15        | 0.48                    | 6                   |
| MXBI (unpublished)  | 182       | 0.19 (0.16 for N = 15)* | 24 (30 for N = 15)* |
| X-ray MXD (from Luckman and Wilson (2005))  | 78        | 0.49                    | 6                   |

322 *\*The RBAR and EPS values in parentheses are for the original ring-width and MXBI time-series*  
 323 *computed for exactly the same 15 trees that have been used to produce the wood anatomy datasets.*

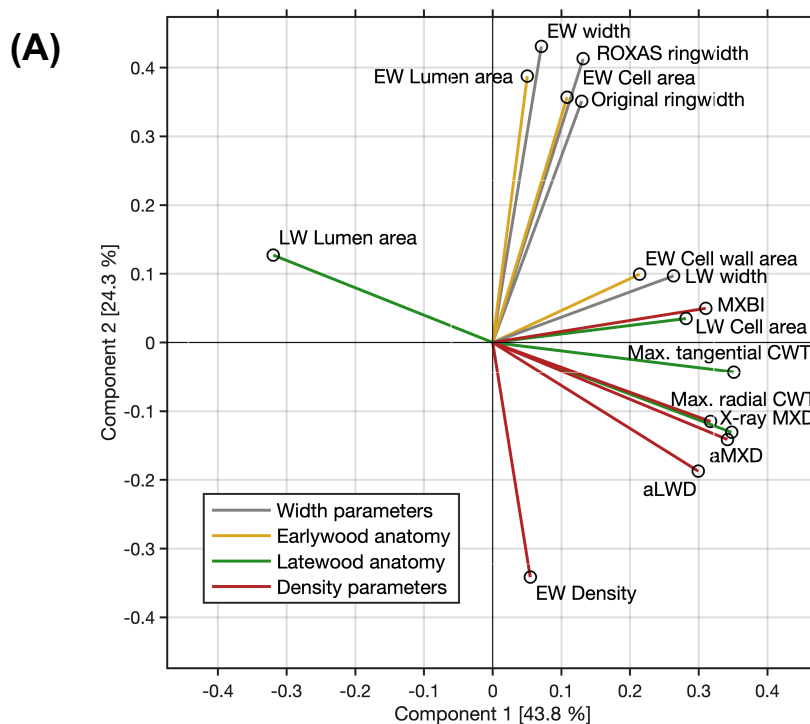
324

325 The co-variability between the various parameters over their common 1700–1994 period was  
 326 assessed through principal component analysis and pairwise correlations (fig. 3). The first two  
 327 components together represent 68.1% of the total variation. The PC1 alone explains 43.8% of  
 328 variance, and is dominated by latewood-related parameters, including both anatomy and  
 329 density parameters. We found that aMXD, Max. radial CWT and X-ray MXD cluster together  
 330 in the bivariate plot, showing that all three parameters express comparable signals (also  
 331 corroborated by the correlation matrix in fig. 3b). The MXBI also loads strongly positively on  
 332 PC1, but slightly separates from this cluster by being positively correlated to PC2. Among the  
 333 LW density-related components, MXBI is the parameter best correlated with ring-width and  
 334 latewood-width chronologies (fig. 3b), although these correlations are only moderate ( $r_{\text{MXBI vs.}}$   
 335  $\text{original ring width} = 0.43$ ,  $r_{\text{MXBI vs. latewood width}} = 0.66$ ). The principal component analysis including the

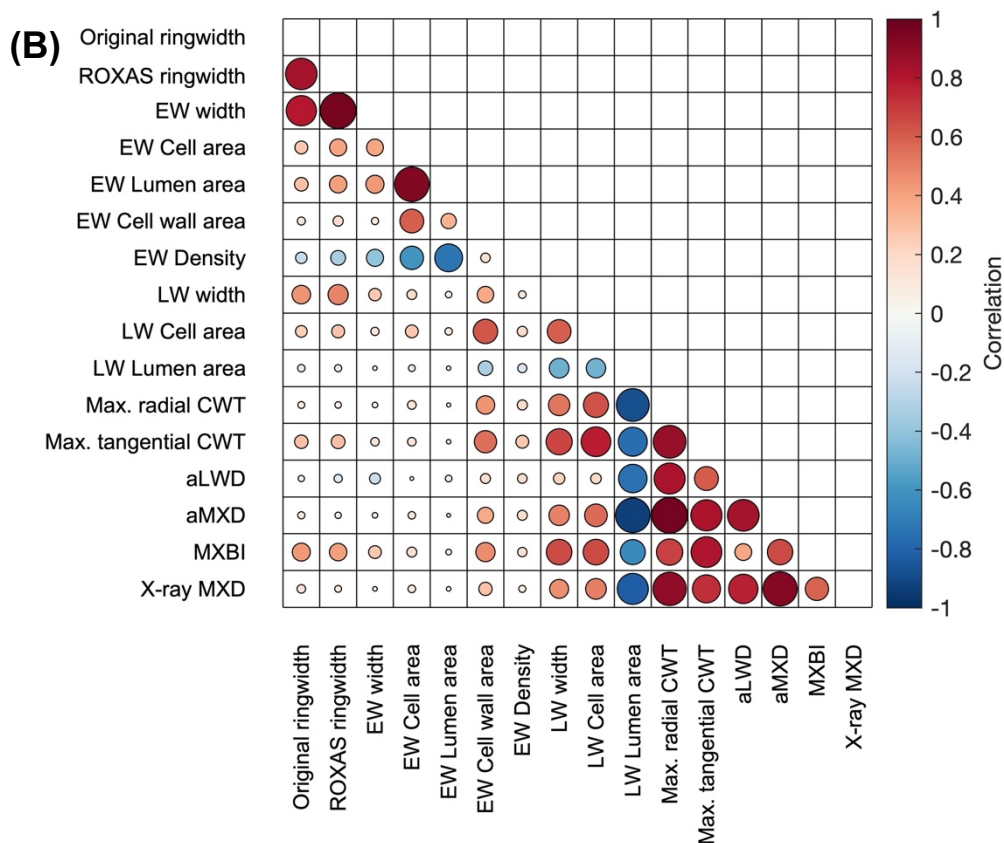
336 subsampled MXBI percentile chronologies based on the *absolute* corresponding ring widths  
 337 reveal that the correlation coefficients against the latewood width, and to some degree also  
 338 ring width, successively increase for the “narrow-ring MXBI chronologies” (fig. S5). The “wide-  
 339 ring MXBI chronologies” (i.e., ~50<sup>th</sup>-100<sup>th</sup> percentiles) are, on the other hand, more similar to  
 340 the aLWD, Max. radial CWT, aMXD and X-ray MXD chronologies. This observed ring-width  
 341 inclination of MXBI suggest that the dataset might be subject to a resolution bias (Björklund et  
 342 al. 2019). More [detail on this](#) issue in [sect. 3.4](#).

343

344 The variance of PC2 (24.3 % of total variability) is dominated by ring width and earlywood-  
 345 related density and anatomy parameters. Amongst these, EW density stands out by loading  
 346 strongly negatively on the PC2 axis (reflecting its negative association with early-summer  
 347 temperatures, see [sect. 3.2](#)). Moreover, the EW cell wall area stands out by loading more  
 348 strongly on the PC1 axis than on the PC2 axis, and by clustering more closely with the  
 349 latewood than with the earlywood components (reflecting its late-summer temperature  
 350 sensitivity, see [sect. 3.2](#)).



351



352

353 **Figure 3:** A) biplot of the first two principal components of the PCA performed 1700–1994 CE  
 354 period on the width, anatomy and density parameters. The colors of the vectors correspond  
 355 to the parameter grouping used in table 1. The first two components together represent 68.1%  
 356 of the total variation. B) Pearson's correlation matrix between various anatomical and width  
 357 parameters. X-ray MXD and MXBI are included for comparison. Correlations are computed  
 358 over the common 1700–1994 period using detrended chronologies. The color and size of the  
 359 markers denote the direction and strength of the relationships.

360

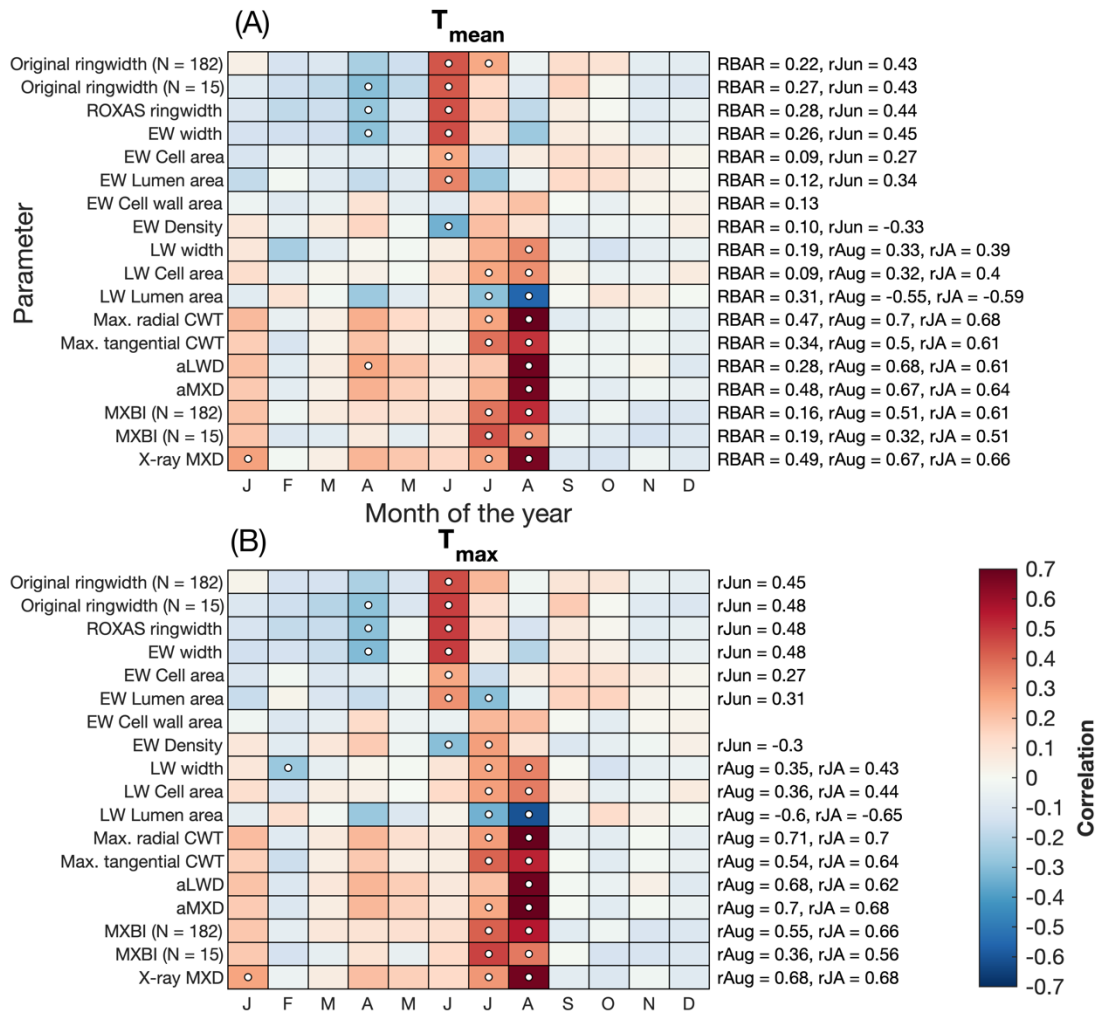
### 361 3.2 Climate response

362 Simple linear correlations between selected parameters and monthly CRU TS mean (Tmean)  
 363 and maximum (Tmax) detrended temperatures are shown in [fig. 4](#). In line with previous work  
 364 from North America (Harley et al. 2021; Heeter et al. 2021; Luckman and Wilson 2005; Wilson  
 365 et al. 2014; Wilson and Luckman 2003), our results reinforce the importance of Tmax  
 366 temperatures for wood formation and growth of *P. engelmannii* in the region by providing, in  
 367 general, slightly higher correlation values for Tmax than for Tmean. Interestingly, the pattern  
 368 observed in North America contrasts to many other temperature-limited regions of the  
 369 Northern Hemisphere, where conifers have generally been noted to correlate stronger to  
 370 Tmean than to Tmax (observation made by the author team, results not published). Whether

371 this is actually grounded in a tree physiological mechanism is still an open question.  
372 Furthermore, the general pattern revealed by the climate response analysis shows that the  
373 various dendroanatomical traits respond to consecutive temporal windows within a short  
374 seasonal window extending from June to August, in line with our understanding of the  
375 successive physiological processes (i.e., cell expansion and cell wall thickening) behind wood  
376 formation and growth (e.g., Fonti et al. 2013). These results support the climate-response  
377 pattern that has generally been observed for conifers across the Canadian Rockies (Luckman  
378 and Wilson 2005) and the adjacent Interior British Columbia (Wilson et al. 2014; Wilson and  
379 Luckman 2003), yet contrasts to the seasonally wide temperature imprint (extending between  
380 May–August and occasionally even between April–September) within latewood density of  
381 black spruce in the eastern Canadian taiga (Wang et al. 2020). This is also the case when  
382 comparing our results with the previous study of (Björklund et al. 2020) on latewood  
383 anatomical traits of *P. sylvestris* in northern Scandinavia, where the temperature response  
384 window extends from April to September. The narrow window of response patterns seen here  
385 is most likely constrained by the distinct and short warm season characterizing the climatology  
386 of the study site, where average monthly temperatures rise above 0 °C only in five months of  
387 the year (fig. 1c).

388

389 We find that latewood-related parameters in general display a late-summer (July–August)  
390 temperature sensitivity, while ring width and earlywood-related density and anatomy  
391 parameters most strongly correlate with mid-summer (June–July) temperatures (fig. 4). The  
392 strongest temperature signals are found in anatomical components of the latewood, which are  
393 also the parameters displaying the highest RBAR statistics (table 1). In particular, aMXD and  
394 Max. radial CWT stand out. The imprints of year-to-year temperature variability within these  
395 two parameters are, over the 1901–1994 period, very similar, if not identical, to that of the  
396 MXD derived from the X-ray technique. By comparison, the exceptionally weak inter-series  
397 signal strength of the MXBI parameter (table 1) is compensated by high replication (N = 182),  
398 and thus MXBI is also rather similar to aMXD, Max. radial CWT and X-ray MXD. However, the  
399 temperature signal of MXBI is shifted earlier by expressing stronger correlation with July  
400 temperatures but weaker with August compared to aMXD, Max. radial CWT and X-ray MXD.  
401 The aggregated July–August temperature response of MXBI is thus in fact only marginally  
402 weaker than that of X-ray MXD, aMXD and Max. radial CWT.



403

404 **Figure 4:** Correlations between tree-ring parameters and monthly (A) average ( $T_{mean}$ ) and (B)  
 405 maximum ( $T_{max}$ ) temperatures from the CRU TS v4.03 product (48.25–55.75° N/113.75–  
 406 123.25° W subset average). Pearson's correlation coefficients are computed over the 1901–  
 407 1994 period using detrended data. The RBAR statistics for each parameter chronology, and  
 408 correlation coefficients for the best temperature target season are provided on the right side  
 409 of the plots (June for ring width and EW parameters, July-August and August for LW  
 410 parameters). For original ring width and MXBI, results are also provided for chronologies  
 411 (denoted as N = 15) built from the same 15 trees that are used to produce the dendroanatomy  
 412 data. Significant correlations ( $p < 0.01$ ) are marked with white circles. Correlations with  
 413 temperature data produced by the Meteorological Service of Canada are given in the  
 414 supplement (fig. S2).

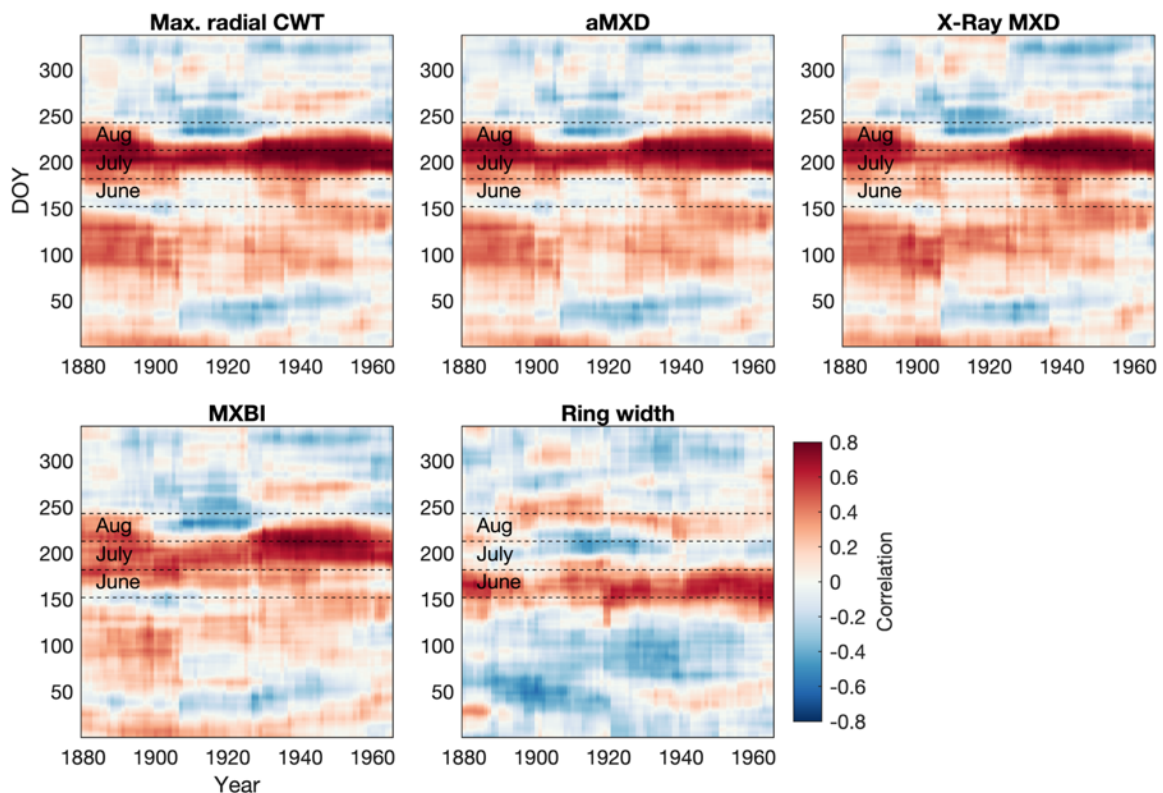
415

### 416 3.3 Temporal signal stability

417 Focusing only on anatomical traits with the highest temperature sensitivity (aMXD and Max.  
 418 radial CWT), comparison against daily temperatures (fig. 5) confirms a significant and strong  
 419 mid/late summer signal over the 1880–1994 period. Breaking down the climate response in



420 daily increments reveals that the strongest signal ( $r > 0.5$ ) occurs on average between day  
 421 192 and day 251 of the year (i.e. July 11<sup>th</sup> until September 8<sup>th</sup>-9<sup>th</sup>, with a peak correlation of  
 422 0.74 for Max. radial CWT and aMXD occurring between 21<sup>st</sup> of July-20<sup>th</sup> of Aug and 23<sup>rd</sup> of  
 423 July-22<sup>nd</sup> of August), respectively. The temperature associations at the margins of the target  
 424 season are, however, more unstable. We note, for example, that the September signal  
 425 disappears around the first half of the 20<sup>th</sup> century for both anatomical parameters. A similar  
 426 correlation structure holds for X-ray derived MXD and to a lesser degree MXBI (N = 182), but  
 427 the two parameters exhibit enhanced correlation coefficients in the second half of the 20<sup>th</sup>  
 428 century compared to the early period (also corroborated by the split-period calibration in [figure](#)  
 429 [6](#)). Moreover, despite the high sample replication, MXBI shows slightly weaker correlations  
 430 with daily data than the other density-related parameters, particularly in the early 1880–1930  
 431 period, when ring widths coincidentally are the narrowest in the record (see [fig. 8](#) and [sect.](#)  
 432 [3.4](#)). For comparative purposes we also include anatomically derived ring width, which shows,  
 433 on average, the strongest correlations ( $r = 0.3$  to  $0.5$ ) with temperatures between day 146 and  
 434 206 of the year (i.e. May 26<sup>th</sup> to July 25<sup>th</sup>).

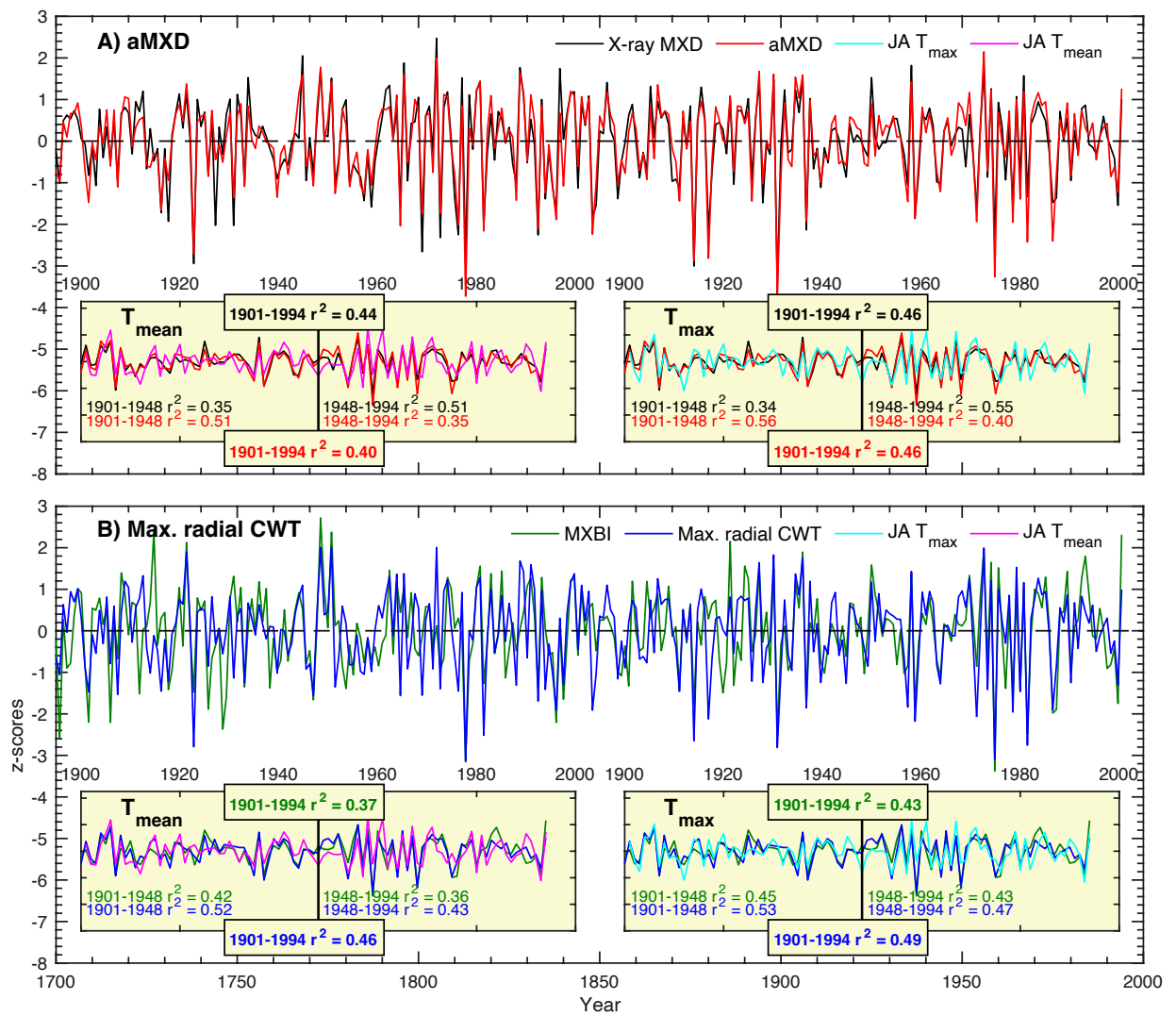


435  
 436 **Figure 5:** Moving correlation between the full tree-ring parameter datasets and Berkeley Earth  
 437 gridded daily temperatures (grid 52.5°N 118.5°W, 1880–1994 period). A 30-year moving  
 438 window, shifted by one year, was used in the analysis. Temperatures were averaged over a  
 439 30-day window and shifted throughout the year at daily steps. The days on the x- and y-axis  
 440 thus show the first day of the 30-year and 30-day windows, respectively. E.g., day 152 on the

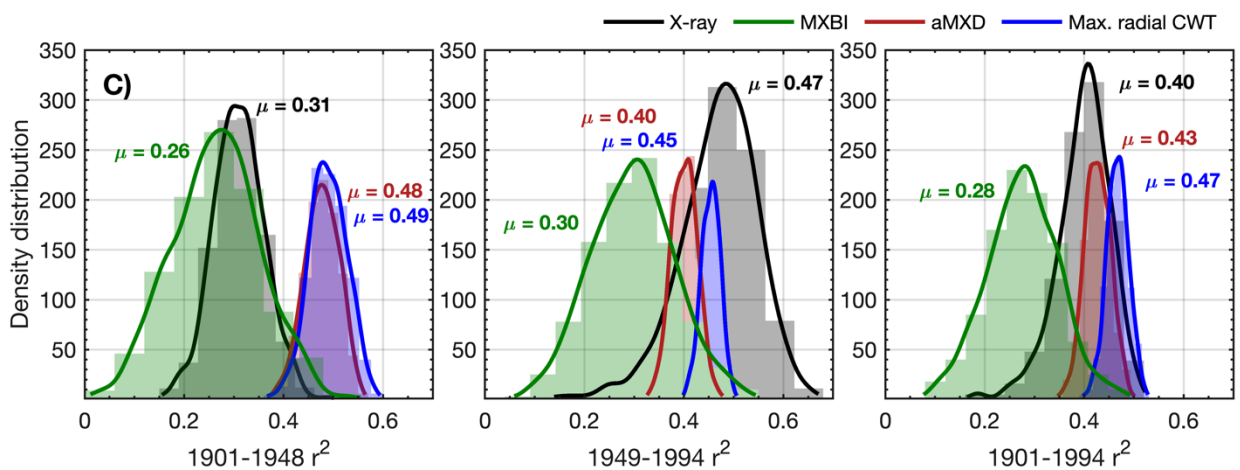
441 y-axis represents the period from June 1 to June 30. Both tree-ring and temperature data have  
442 been detrended prior to analysis. The June-August months are highlighted to aid  
443 interpretation. Pearson's correlations between monthly aggregated (i.e. average daily data for  
444 each calendar month) Berkeley Earth temperatures and tree-ring parameters are provided in  
445 figure S6 for comparison.  
446

447 The stability of the July-August temperature signals of detrended aMXD and Max. radial CWT,  
448 along with X-ray MXD and MXBI, were further assessed by a split-period calibration procedure  
449 (1901–1948 and 1949–1994) (fig. 6). The two wood anatomical parameters calibrate more  
450 strongly to the early period compared to the late, both when using Tmean and Tmax. However,  
451 especially for Max. radial CWT, the calibration differences in the two periods are slight ( $r^2 =$   
452 53% and 47% against Tmax, respectively). By comparison, the X-ray MXD calibrate more  
453 strongly in the latter half of the instrumental period and show more pronounced temporal  
454 instabilities ( $r^2 = 34%$  and 55% against Tmax, respectively). This contrasts to the prior finding  
455 (Luckman and Wilson 2005), where no such instabilities in the early 20<sup>th</sup> century were  
456 detected. These contrasting results are most likely not related to using different climate data  
457 products because similar results (fig. S3) were obtained when using the Luckman and Wilson  
458 (2005) temperature data, originally produced by the Meteorological Service of Canada.  
459 Instead we suspect that the discrepancy can be attributed to either using a larger network of  
460 MXD data than used in this study, or that Luckman and Wilson (2005) used multivariate  
461 regression models (including ring width and lagged growth responses) to explain a wider target  
462 season than attempted here.  
463

464 Calibration trials with detrended data over the full period 1901–1994 reveal that Max. radial  
465 CWT performs overall best (Tmax  $r^2 = 49%$ ), closely followed by aMXD ( $r^2 = 0.46%$ ) and X-  
466 ray MXD ( $r^2 = 0.46%$ ). The temporal instability of X-ray MXD and by comparison the robust  
467 and strong signals of the aMXD and especially the Max. radial CWT parameters are further  
468 confirmed by the resampling calibration trials presented in fig. 6c, where 10 random series are  
469 drawn from the sample cohorts 1000 times without replacement, and the resulting parameter  
470 chronologies are subsequently correlated against July-August Tmax. The reason for the X-ray  
471 MXD loss in signal is difficult to disentangle, but it is unlikely related to having different samples  
472 for the X-ray and anatomical datasets because the resampling scheme clearly show that the  
473  $r^2$ -distributions are different (fig. 6c) (also corroborated by a two-sample t-test at a significance  
474 threshold of 0.05, indicating that the  $r^2$ -statistics comes from two populations with unequal  
475 means).



476



477

478 **Figure 6:** A-B): Full (1901–1994) and split-period (1901–1948, 1949–1994) calibration  
 479 statistics for the Max. radial CWT (blue line), aMXD (red line), X-ray MXD (black line) and  
 480 MXBI (green line) chronologies against July-August mean and maximum CRU TS

481 temperature. Time-series in the figures show non-detrended mean chronologies, z-scored  
482 over the instrumental 1901–1994 period. C): The density distribution of  $r^2$ -values obtained from  
483 1000 calibration trials where parameter chronologies are built from 10 series randomly drawn  
484 without replacement from the sample cohort. The resampling trials are based on *detrended*  
485 climate and tree-ring data. Calibrations are performed against July-August maximum  
486 temperatures.

487

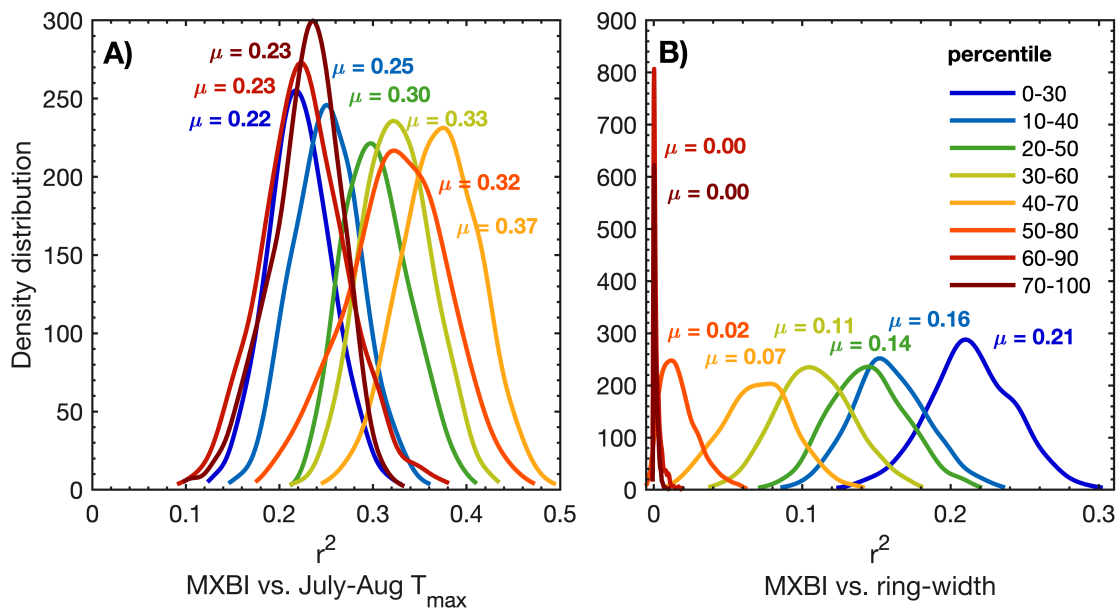
### 488 3.4 Possible implications of measurement resolution on climate signal

489 As shown in the previous sections, the climate imprint withing the anatomical LW density  
490 components slightly differs from its X-ray and BI based counterparts, although all these  
491 parameters essentially measure the same component in wood. As previously noted by  
492 Björklund et al. (2020), the main difference between these metrics is the measurement  
493 resolution, while factors such as the cell wall density is of marginal importance (Björklund et  
494 al. 2021). Thus, as part of a multi-parameter approach, the higher resolution of dendroanatomy  
495 may serve to evaluate the potential risk of a resolution bias (in X-ray MXD and MXBI) when  
496 implementing these parameters both on shorter and longer timescales.

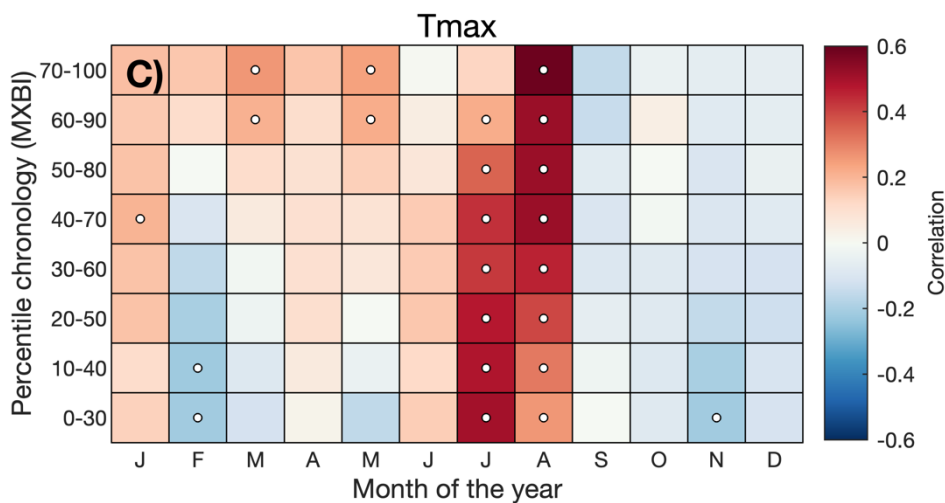
497

498 We have seen that the monthly correlations of the full MXBI dataset (N = 182) differ slightly  
499 from the more physically direct density and anatomy parameters, which we hypothesize could  
500 partially be related to the lower measurement resolution that artificially makes it more similar  
501 to ring width and latewood width (Björklund et al., 2019). The pairwise correlation between  
502 parameter chronologies (fig. 3) and the PCA biplot based on the percentile MXBI chronologies  
503 (fig. S5) confirms this enhanced relationship with ring width/latewood width. To test this theory  
504 further, we have correlated the percentile MXBI chronologies against the target July-August  
505 Tmax (fig. 7a) and against the full (N = 182) detrended original ring-width chronology (fig. 7b),  
506 using resampling of data. Unfortunately, corresponding latewood width measurements are not  
507 available for MXBI, so this comparative analysis is restricted to ring width. Nevertheless, we  
508 find that when using the full July-August season the poorest temperature imprint is found in  
509 the MXBI values of the narrowest (~40%), *and* the widest (~40%) of the rings, while the  
510 strongest July-August signal can be recovered from the MXBI-values in rings that are close to  
511 average in width (40<sup>th</sup> – 70<sup>th</sup> percentile). Expanding the climate correlation analysis to monthly  
512 Tmax data (fig. 7c) reveals, however, a gradual transition from predominantly an August  
513 temperature signal in the wide ring MXBI chronologies to a more July dominated signal in the  
514 narrow ring MXBI chronologies. MXBI-values in rings that are close to average in width  
515 correlate equally strong to both July and August, which explains the overall better performance  
516 of these data when comparing to the July-August target (fig. 7c). Importantly, we find no  
517 correlation between the MXBI and ring-width in the widest rings (fig. S5). However, as we

518 move towards narrower rings, the MXBI-values become successively more like ring  
 519 width/latewood width (fig. 7b and fig. S5). All in all, these results suggest that an effect of low  
 520 measurement resolution may be present for narrower ring widths/latewood widths. If so, this  
 521 means that the MXBI parameter may become subject to greater target seasonal uncertainty,  
 522 which may fluctuate between July and August signals through time, largely depending on the  
 523 absolute ring width/latewood width of the analyzed tree-ring sample collection and the  
 524 resolution of the captured image. Although posing a challenge for paleoclimate  
 525 reconstructions, this resolution issue is likely to become a less relevant methodological  
 526 problem in a near future, as more laboratories are currently investing in the development of  
 527 high-resolution image capturing systems and other analytical techniques to enhance the  
 528 precision of the BI data.



529



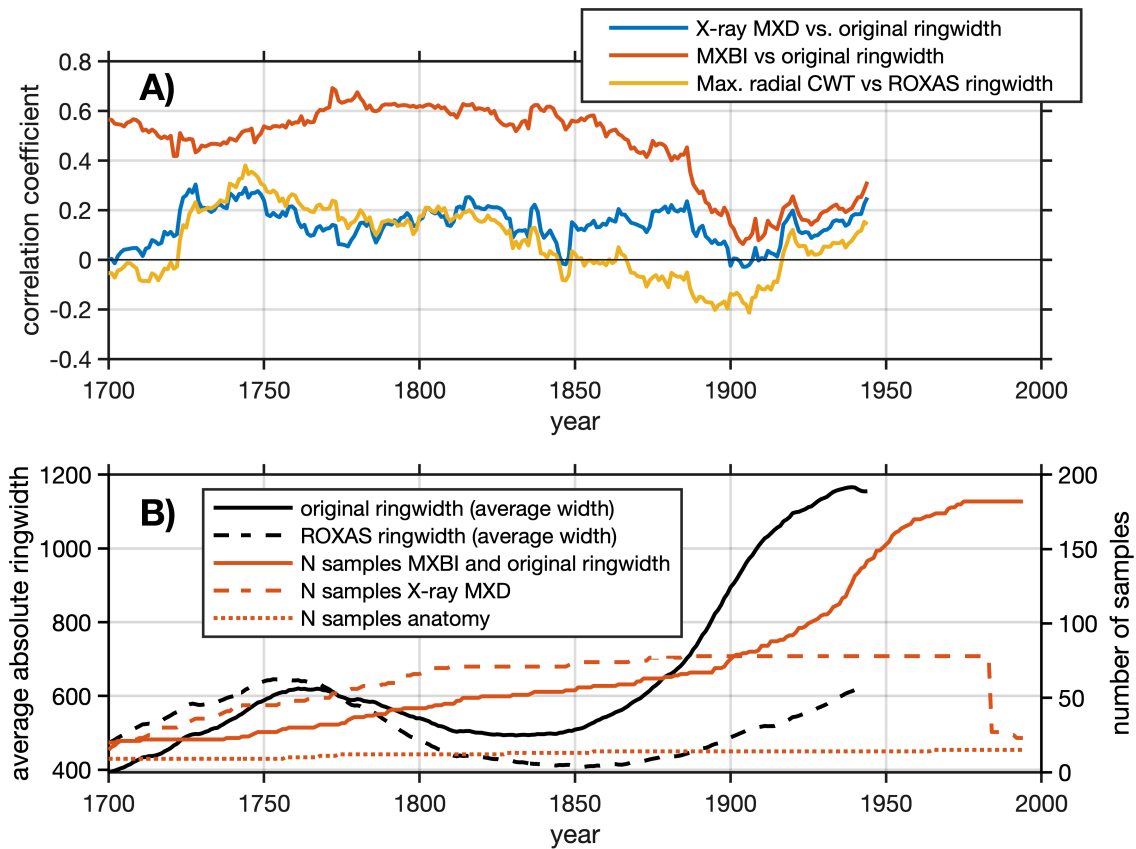
530

531 **Figure 7:** A)-B): The density distribution of  $r^2$ -values obtained from 1000 calibration trials  
 532 (1901–1994 period) where MXBI chronologies are built from 100 series randomly drawn from  
 533 the total of 182 series without replacement. The detrended MXBI values are sorted into

534 percentiles based on the absolute ring-width (e.g., the 0-30 percentile are the corresponding  
535 MXBI-values for the narrowest 30% of the rings), and then averaged into percentile  
536 chronologies. A) the calibration  $r^2$ -values between these chronologies and detrended July-  
537 August CRU TS Tmax, B) same as A) but calibrated against the full ( $N = 182$ ) detrended ring-  
538 width chronology. C) Correlation between the MXBI percentile chronologies and monthly  
539 maximum (Tmax) temperatures from the CRU TS v4.03 product ( $48.25\text{--}55.75^\circ\text{ N}/113.75\text{--}$   
540  $123.25^\circ\text{ W}$  subset average). Correlation coefficients are computed over the 1901–1994 period  
541 using detrended tree-ring and temperature data. Significant correlations ( $p < 0.01$ ) are outlined  
542 with white circles.

543  
544 Further, we note that the correlations between the various latewood parameters against ring  
545 widths change from the early to late 20<sup>th</sup> century periods, and that the correlations slightly  
546 differ in magnitude and sign (fig. 8). The MXBI is positively correlated with ring width, whereas  
547 the correlations for X-ray MXD range from non-significant to weakly positive. The Max. radial  
548 CWT, on the other hand, show a non-significant or weak negative correlation with ring width  
549 during the 20<sup>th</sup> century. This gradual, and slightly larger shift in moving window correlation  
550 against ring width during the early 20<sup>th</sup> century may thus be an indication that both MXBI and  
551 to some degree X-ray MXD are challenged by comparatively low measurement resolution. If  
552 this is the case, then the inter-annual climate signal may potentially become muted when ring  
553 (latewood) widths are narrow. This dependence could, in fact, affect the lower frequencies,  
554 and inflate multi-decadal variability (Esper et al. 2015). Moreover, the fidelity to the monthly  
555 temperature targets may exhibit instability when rings (latewoods) are narrow, shifting back  
556 and forth between August or July dominated signals (as seen in fig. 7c). It is at the moment  
557 unclear how this phenomenon could affect the lower frequencies of our chronologies, as a  
558 robust picture of long-term trends in dendroanatomical parameters can only emerge from  
559 analysis of millennial length, multi-generation, composite chronologies suitable for RCS-type  
560 detrending (Briffa and Melvin 2011). Moreover, periods with persistence in narrow ring widths  
561 will force MXBI, and perhaps also X-ray MXD, to exhibit persistently low densitometric values  
562 (Björklund et al. 2019). Exacerbating this issue is that persistently narrow ring width/latewood  
563 width may not even be a product of the distinct and earlier temperature target (June-July, fig.  
564 4), but could also be related to stand dynamics/disturbances (Rydval et al. 2018), and thus  
565 pass down non-climatic distortions of decadal to centennial variations to X-ray MXD and MXBI.  
566 This clearly needs further scrutiny because it may be important for the interpretation of inferred  
567 climate signals back in time, particularly because the ring-width correlation converges for the  
568 X-ray and anatomy data but dramatically diverges for MXBI (fig. 8). The lower late-period  
569 (1949–1994) signal of the anatomical parameters compared to X-ray MXD requires a different  
570 explanation (fig. 6). According to the distribution of the  $r^2$ -values in the resampling scheme of

571 figure 6c, the late period Tmax signals are not appreciably different, so perhaps this is simply  
 572 by chance compounded by having five times higher X-ray MXD replication.



573  
 574 **Figure 8:** A) running *Pearson's* correlation (a 50-year window shifted by one year) between  
 575 selected density parameters and ring width. The years on the x-axis show the first year of the  
 576 50-year correlation windows. Note that for X-ray MXD, the ring-width data are not obtained  
 577 from the same tree cores as have been used for the density measurements, which is otherwise  
 578 the case for both MXBI and anatomy. B) running average of absolute ring widths (original and  
 579 ROXAS datasets) computed using a 50-year window shifted by one year, together with the  
 580 chronology sample depths of the X-ray MXD, MXBI and dendroanatomical datasets.

581  
 582 **Concluding remarks**

583 Tree-ring based reconstructions of pre-industrial climate provide a key insight into Earth's  
 584 present and future changing climate, yet their full potential will remain unexploited without a  
 585 concerted effort to overcome several critical challenges. This study is part of a larger ongoing  
 586 synergetic effort (e.g., Björklund et al. 2020, and other work currently in preparation) directed  
 587 at exploring the efficacy of highly temperature sensitive tree-ring data frequently used in large  
 588 scale temperature reconstructions (e.g., Wilson et al. 2016), with the ambition to improve upon  
 589 these existing records using dendroanatomical techniques. This is because dendroanatomy  
 590 represents the direct morphological refinement of current microdensitometric techniques

591 where it is possible to control within-ring specific location of the measurements down to the  
592 cellular level (von Arx and Carrer 2014).

593  
594 In summary, based on the collective comparison between the new wood anatomical dataset  
595 of *P. engelmannii* from the Columbia Icefields and the two predecessors X-ray MXD and MXBI,  
596 we are able to draw the following conclusions:

597 1. Maximum radial cell wall thickness and anatomical MXD are the two most promising  
598 wood anatomical proxy parameters for estimating past temperatures, each explaining  
599 >45% in instrumental detrended July-August maximum temperatures. Both  
600 parameters display a comparable climatic imprint and strength of signal to the X-ray  
601 derived MXD. It does, however, appear that the stability of the temperature signal over  
602 time is more robust for the maximum radial cell wall thickness than for X-ray MXD.

603 2. For these anatomical parameters, the number of trees needed to reach the commonly  
604 accepted quality threshold for chronologies used in dendroclimatic analyses is, for our  
605 experimental site and species, exemplary with just six trees. However, this high  
606 common signal strength is matched by the X-ray MXD parameter and thus does not  
607 constitute an obvious advantage by itself. Nevertheless, if the temperature signal is  
608 more stable in maximum radial cell wall thickness, it is advantageous to know that very  
609 few trees are needed to reach chronology confidence. This is especially true given that  
610 the problem of fading records, i.e. the general decrease in sample replication and  
611 between tree correlations back in time (Esper and Büntgen 2021), poses a severe  
612 constraint to almost all chronologies extending up to or beyond the last millennium.

613 3. The higher resolution of dendroanatomy appears to positively influence the high-  
614 frequency temperature signal stability. Using anatomical parameters as opposed to  
615 density parameters, be it from X-ray or anatomy, may also be beneficial for data quality  
616 and the mechanistic interpretation of the proxy record. However, further research is  
617 needed to consolidate this and other important potential effects regarding the low  
618 frequency fidelity of long-term temperature reconstructions based on X-ray  
619 densitometry.

620  
621 Justification of the cost and time constraints currently associated to the production of long  
622 dendroanatomical datasets requires that there must be an information gain not obtainable  
623 from conventional techniques. In fact, high-resolution, cell-based, measurements already offer  
624 an advantage when it comes to the understanding of the structure – function relationships  
625 (e.g., Bouche et al. 2014; Pittermann et al. 2011; Wilkinson et al. 2015), the complex  
626 mechanisms behind tree-ring formation (Rathgeber et al. 2016), with relative timestamps  
627 (Ziaco 2020) of brief intra-seasonal climate extremes, such as late growing season cold spells



628 or initiation of volcanic cooling episodes (Edwards et al. 2022; Piermattei et al. 2020). The  
629 question remains, however, whether dendroanatomy can also provide additional paleoclimate  
630 information. Despite the encouraging results detailed herein, it is necessary to continue to  
631 extend this dataset by adding more series from multiple age classes across the last millennium  
632 to more thoroughly evaluate the multi-centennial to millennial scale variations of this key  
633 temperature proxy site. The work detailed here is the first piece of a puzzle to explore  
634 dendroanatomy of the *P. engelmannii* sample set for the Columbia Icefield area in Canada,  
635 formerly analyzed with X-ray and BI techniques (Luckman and Wilson 2005). As such, it also  
636 represents the longest (1585–2014 CE) dendroanatomical dataset currently developed for  
637 North America.

638

### 639 **Author contributions**

640 KS and JB conceptualized the research and obtained the funding to support it. MF performed  
641 the dendroanatomical measurements, using wood material collected by BL and RW. GvA  
642 aided the interpretation of the dendroanatomical data, and MR of the BI-measurements. KS  
643 carried out the analysis and drafted the paper. All authors contributed to the planning and  
644 structuring of the paper.

645

### 646 **Data availability**

647 The dendroanatomical chronologies from the Icefields area, Canada, will be available on  
648 request.

649

### 650 **Competing interests**

651 The authors declare that they have no conflict of interest.

652

### 653 **Acknowledgments**

654 This work was financed by FORMAS (Grant No. 2019-01482 to KS), the Swiss National  
655 Science Foundation (Project XELLCLIM no. 200021\_182398 to GvA.) RW received funds  
656 through the US National Science Foundation (NSF) Grant AGS 1502150 for the MXBI  
657 measurements. MR was supported by the Czech Science Foundation project REPLICATE  
658 (20-22351Y).

659

### 660 **References**

661 Anchukaitis KJ et al. (2017) Last millennium Northern Hemisphere summer temperatures  
662 from tree rings: Part II, spatially resolved reconstructions Quaternary Science Reviews  
663 163:1-22 doi:<https://doi.org/10.1016/j.quascirev.2017.02.020>

664 Björklund J, Fonti MV, Fonti P, Van den Bulcke J, von Arx G (2021) Cell wall dimensions reign  
665 supreme: cell wall composition is irrelevant for the temperature signal of latewood  
666 density/blue intensity in Scots pine *Dendrochronologia* 65  
667 doi:10.1016/j.dendro.2020.125785

668 Björklund J, Seftigen K, Fonti P, Nievergelt D, von Arx G (2020) Dendroclimatic potential of  
669 dendroanatomy in temperature-sensitive *Pinus sylvestris* *Dendrochronologia* 60  
670 doi:10.1016/j.dendro.2020.125673

671 Björklund J et al. (2019) Scientific merits and analytical challenges of tree-ring densitometry  
672 *Reviews of Geophysics* 57:1224-1264 doi:10.1029/2019RG000642

673 Blake SAP, Palmer JG, Björklund J, Harper JB, Turney CSM (2020) Palaeoclimate potential of  
674 New Zealand *Manoao colensoi* (silver pine) tree rings using Blue-Intensity (BI)  
675 *Dendrochronologia* 60 doi:10.1016/j.dendro.2020.125664

676 Bouche PS, Larter M, Domec J-C, Burlett R, Gasson P, Jansen S, Delzon S (2014) A broad survey  
677 of hydraulic and mechanical safety in the xylem of conifers *Journal of experimental*  
678 *botany* 65:4419-4431 doi:10.1093/jxb/eru218

679 Briffa KR et al. (1992) Fennoscandian summers from ad 500: temperature changes on short  
680 and long timescales *Climate Dynamics* 7:111-119 doi:10.1007/bf00211153

681 Briffa KR, Melvin TM (2011) A Closer Look at Regional Curve Standardization of Tree-Ring  
682 Records: Justification of the Need, a Warning of Some Pitfalls, and Suggested  
683 Improvements in Its Application. In: Hughes MK, Swetnam TW, Diaz HF (eds)  
684 *Dendroclimatology: Progress and Prospects*. Springer Netherlands, Dordrecht, pp 113-  
685 145. doi:10.1007/978-1-4020-5725-0\_5

686 Briffa KR, Osborn TJ, Schweingruber FH, Jones PD, Shiyatov SG, Vaganov EA (2002) Tree-ring  
687 width and density data around the Northern Hemisphere: Part 1, local and regional  
688 climate signals *The Holocene* 12:737-757 doi:10.1191/0959683602h1587rp

689 Cook ER, Peters K (1981) The smoothing spline: a new approach to standardizing forest  
690 interior tree-ring width series for dendroclimatic studies *Tree-Ring Bulletin* 41:45-53

691 Cuny HE, Fonti P, Rathgeber CBK, von Arx G, Peters RL, Frank DC (2019) Couplings in cell  
692 differentiation kinetics mitigate air temperature influence on conifer wood anatomy  
693 *Plant, Cell & Environment* 42:1222-1232 doi:<https://doi.org/10.1111/pce.13464>

694 Cuny HE, Rathgeber CBK, Frank D, Fonti P, Fournier M (2014) Kinetics of tracheid development  
695 explain conifer tree-ring structure *New Phytol* 203:1231-1241 doi:10.1111/nph.12871

696 D'Arrigo R, Wilson R, Jacoby G (2006) On the long-term context for late twentieth century  
697 warming *Journal of Geophysical Research: Atmospheres* 111  
698 doi:<https://doi.org/10.1029/2005JD006352>

699 Denne MP (1989) Definition of Latewood According to Mork (1928) *Iawa J* 10:59-62  
700 doi:<https://doi.org/10.1163/22941932-90001112>

701 Edwards J, Anchukaitis KJ, Gunnarson BE, Pearson C, Seftigen K, von Arx G, Linderholm HW  
702 (2022) The Origin of Tree-Ring Reconstructed Summer Cooling in Northern Europe  
703 During the 18th Century Eruption of Laki *Paleoceanography and Paleoclimatology*  
704 37:e2021PA004386 doi:<https://doi.org/10.1029/2021PA004386>

705 Eschbach W, Nogler P, Schär E, Schweingruber F (1995) Technical advances in the  
706 radiodensitometrical determination of wood density *Dendrochronologia* 13:155-168

707 Esper J, Büntgen U (2021) The future of paleoclimate *Climate Research* 83:57-59

708 Esper J, Cook ER, Schweingruber FH (2002) Low-frequency signals in long tree-ring  
709 chronologies for reconstructing past temperature variability *Science* 295:2250-2253

710 Esper J et al. (2018) Large-scale, millennial-length temperature reconstructions from tree-  
711 rings *Dendrochronologia* 50:81-90 doi:<https://doi.org/10.1016/j.dendro.2018.06.001>  
712 Esper J, Schneider L, Smerdon JE, Schöne BR, Büntgen U (2015) Signals and memory in tree-  
713 ring width and density data *Dendrochronologia* 35:62-70  
714 doi:<http://dx.doi.org/10.1016/j.dendro.2015.07.001>  
715 Fonti P, Bryukhanova MV, Myglan VS, Kirdyanov AV, Naumova OV, Vaganov EA (2013)  
716 Temperature-induced responses of xylem structure of *Larix sibirica* (Pinaceae) from  
717 the Russian Altay *American journal of botany* 100:1332-1343  
718 doi:10.3732/ajb.1200484  
719 Fonti P, von Arx G, Garcia-Gonzalez I, Eilmann B, Sass-Klaassen U, Gartner H, Eckstein D (2010)  
720 Studying global change through investigation of the plastic responses of xylem  
721 anatomy in tree rings *New Phytol* 185:42-53 doi:10.1111/j.1469-8137.2009.03030.x  
722 Frank D, Esper J, Zorita E, Wilson R (2010) A noodle, hockey stick, and spaghetti plate: a  
723 perspective on high-resolution paleoclimatology *Wiley Interdisciplinary Reviews:*  
724 *Climate Change* 1:507-516 doi:10.1002/wcc.53  
725 Franke J, Frank D, Raible CC, Esper J, Bronnimann S (2013) Spectral biases in tree-ring climate  
726 proxies *Nature Clim Change* 3:360-364  
727 Goose H (2017) Reconstructed and simulated temperature asymmetry between continents  
728 in both hemispheres over the last centuries *Climate Dynamics* 48:1483-1501  
729 doi:10.1007/s00382-016-3154-z  
730 Harley GL, Heeter KJ, Maxwell JT, Rayback SA, Maxwell RS, Reinemann TEP, H. Taylor A (2021)  
731 Towards broad-scale temperature reconstructions for Eastern North America using  
732 blue light intensity from tree rings *International Journal of Climatology* 41:E3142-  
733 E3159 doi:<https://doi.org/10.1002/joc.6910>  
734 Harris I, Osborn TJ, Jones P, Lister D (2020) Version 4 of the CRU TS monthly high-resolution  
735 gridded multivariate climate dataset *Scientific Data* 7:109 doi:10.1038/s41597-020-  
736 0453-3  
737 Heeter KJ et al. (2021) Summer temperature variability since 1730 CE across the low-to-mid  
738 latitudes of western North America from a tree ring blue intensity network *Quaternary*  
739 *Science Reviews* 267:107064 doi:<https://doi.org/10.1016/j.quascirev.2021.107064>  
740 Jevsenak J, Levanic T (2018) dendroTools: R package for studying linear and nonlinear  
741 responses between tree-rings and daily environmental data *Dendrochronologia*  
742 48:32-39 doi:10.1016/j.dendro.2018.01.005  
743 Konter O, Büntgen U, Carrer M, Timonen M, Esper J (2016) Climate signal age effects in boreal  
744 tree-rings: Lessons to be learned for paleoclimatic reconstructions *Quaternary Science*  
745 *Reviews* 142:164-172 doi:<https://doi.org/10.1016/j.quascirev.2016.04.020>  
746 Ljungqvist FC et al. (2020) Assessing non-linearity in European temperature-sensitive tree-  
747 ring data *Dendrochronologia* 59 doi:10.1016/j.dendro.2019.125652  
748 Lücke LJ, Hegerl GC, Schurer AP, Wilson R (2019) Effects of Memory Biases on Variability of  
749 Temperature Reconstructions *Journal of Climate* 32:8713-8731 doi:10.1175/jcli-d-19-  
750 0184.1  
751 Luckman BH (1997) DEVELOPING A PROXY CLIMATE RECORD FOR THE LAST 300 YEARS IN THE  
752 CANADIAN ROCKIES – SOME PROBLEMS AND OPPORTUNITIES *Climatic Change*  
753 36:455-476 doi:10.1023/A:1005376713554  
754 Luckman BH (2000) The Little Ice Age in the Canadian Rockies *Geomorphology* 32:357-384  
755 doi:[https://doi.org/10.1016/S0169-555X\(99\)00104-X](https://doi.org/10.1016/S0169-555X(99)00104-X)

756 Luckman BH, Briffa KR, Jones PD, Schweingruber FH (1997) Tree-ring based reconstruction of  
757 summer temperatures at the Columbia Icefield, Alberta, Canada, AD 1073-1983 *The*  
758 *Holocene* 7:375-389 doi:10.1177/095968369700700401

759 Luckman BH, Wilson RJS (2005) Summer temperatures in the Canadian Rockies during the last  
760 millennium: a revised record *Climate Dynamics* 24:131-144 doi:10.1007/s00382-004-  
761 0511-0

762 Luterbacher J et al. (2016) European summer temperatures since Roman times *Environmental*  
763 *Research Letters* 11:024001

764 Mann ME, Bradley RS, Hughes MK (1999) Northern hemisphere temperatures during the past  
765 millennium: Inferences, uncertainties, and limitations *Geophysical Research Letters*  
766 26:759-762 doi:<https://doi.org/10.1029/1999GL900070>

767 McCarroll D, Pettigrew E, Luckman A, Guibal F, Edouard JL (2002) Blue Reflectance Provides a  
768 Surrogate for Latewood Density of High-latitude Pine Tree Rings Arctic, Antarctic, and  
769 Alpine Research 34:450-453 doi:10.1080/15230430.2002.12003516

770 Pacheco A, Camarero JJ, Carrer M (2018) Shifts of irrigation in Aleppo pine under semi-arid  
771 conditions reveal uncoupled growth and carbon storage and legacy effects on wood  
772 anatomy *Agricultural and Forest Meteorology* 253-254:225-232  
773 doi:<https://doi.org/10.1016/j.agrformet.2018.02.018>

774 PAGES 2k Consortium (2013) Continental-scale temperature variability during the past two  
775 millennia *Nature Geoscience* 6:339 doi:10.1038/ngeo1797  
776 <https://www.nature.com/articles/ngeo1797#supplementary-information>

777 PAGES 2k Consortium (2017) A global multiproxy database for temperature reconstructions  
778 of the Common Era *Scientific Data* 4:170088 doi:10.1038/sdata.2017.88  
779 <https://www.nature.com/articles/sdata201788#supplementary-information>

780 Pages k-PMIP3 group (2015) Continental-scale temperature variability in PMIP3 simulations  
781 and PAGES 2k regional temperature reconstructions over the past millennium *Clim*  
782 *Past* 11:1673-1699 doi:10.5194/cp-11-1673-2015

783 Phipps SJ et al. (2013) Paleoclimate Data–Model Comparison and the Role of Climate Forcings  
784 over the Past 1500 Years\* *Journal of Climate* 26:6915-6936 doi:10.1175/jcli-d-12-  
785 00108.1

786 Piermattei A et al. (2020) A millennium-long ‘Blue Ring’ chronology from the Spanish Pyrenees  
787 reveals severe ephemeral summer cooling after volcanic eruptions *Environmental*  
788 *Research Letters* 15:124016 doi:10.1088/1748-9326/abc120

789 Pittermann J, Limm E, Rico C, Christman MA (2011) Structure–function constraints of  
790 tracheid-based xylem: a comparison of conifers and ferns *New Phytol* 192:449-461  
791 doi:10.1111/j.1469-8137.2011.03817.x

792 Prendin AL, Petit G, Carrer M, Fonti P, Björklund J, von Arx G (2017) New research perspectives  
793 from a novel approach to quantify tracheid wall thickness *Tree physiology* 37:976–983

794 Rathgeber CB, Cuny HE, Fonti P (2016) Biological Basis of Tree-Ring Formation: A Crash Course  
795 *Front Plant Sci* 7:734 doi:10.3389/fpls.2016.00734

796 Rohde RA, Hausfather Z (2020) The Berkeley Earth Land/Ocean Temperature Record *Earth*  
797 *Syst Sci Data* 12:3469-3479 doi:10.5194/essd-12-3469-2020

798 Rydval M, Druckenbrod D, Anchukaitis KJ, Wilson R (2015) Detection and removal of  
799 disturbance trends in tree-ring series for dendroclimatology *Canadian Journal of*  
800 *Forest Research* 46:387-401 doi:10.1139/cjfr-2015-0366

801 Rydval M et al. (2018) Influence of sampling and disturbance history on climatic sensitivity of  
802 temperature-limited conifers The Holocene 28:1574-1587  
803 doi:10.1177/0959683618782605

804 Rydval M, Larsson L-Å, McGlynn L, Gunnarson BE, Loader NJ, Young GHF, Wilson R (2014) Blue  
805 intensity for dendroclimatology: Should we have the blues? Experiments from  
806 Scotland Dendrochronologia 32:191-204 doi:10.1016/j.dendro.2014.04.003

807 Schneider L, Smerdon JE, Büntgen U, Wilson RJS, Myglan VS, Kirilyanov AV, Esper J (2015)  
808 Revising midlatitude summer temperatures back to A.D. 600 based on a wood density  
809 network Geophysical Research Letters 42:4556-4562 doi:doi:10.1002/2015GL063956

810 Schweingruber F, Fritts H, Bräker O, Drew L, Schär E (1978) The X-ray technique as applied to  
811 dendroclimatology Tree-Ring Bulletin

812 Seftigen K, Goosse H, Klein F, Chen D (2017) Hydroclimate variability in Scandinavia over the  
813 last millennium – insights from a climate model–proxy data comparison Clim Past  
814 13:1831-1850 doi:10.5194/cp-13-1831-2017

815 St. George S, Luckman BH (2001) Extracting a paleotemperature record from *Picea*  
816 *engelmannii* tree-line sites in the central Canadian Rockies Canadian Journal of  
817 Forest Research 31:457-470 doi:10.1139/cjfr-31-3-457

818 Stoffel M et al. (2015) Estimates of volcanic-induced cooling in the Northern Hemisphere over  
819 the past 1,500 years Nature Geoscience 8:784 doi:10.1038/ngeo2526  
820 <https://www.nature.com/articles/ngeo2526#supplementary-information>

821 Vincent LA, Gullett D (1999) Canadian historical and homogeneous temperature datasets for  
822 climate change analyses International Journal of Climatology: A Journal of the Royal  
823 Meteorological Society 19:1375-1388

824 von Arx G, Carrer M (2014) ROXAS - a new tool to build centuries-long tracheid-lumen  
825 chronologies in conifers Dendrochronologia 32:290-293  
826 doi:10.1016/j.dendro.2013.12.001

827 von Arx G, Crivellaro A, Prendin AL, Cufar K, Carrer M (2016) Quantitative wood anatomy -  
828 practical guidelines Frontiers in Plant Science 7:781 doi:10.3389/fpls.2016.00781

829 von Storch H, Zorita E, Jones JM, Dimitriev Y, González-Rouco F, Tett SFB (2004)  
830 Reconstructing Past Climate from Noisy Data Science 306:679-682  
831 doi:10.1126/science.1096109

832 Wang F, Arseneault D, Boucher É, Galipaud Gloaguen G, Deharte A, Yu S, Trou-kechout N  
833 (2020) Temperature sensitivity of blue intensity, maximum latewood density, and ring  
834 width data of living black spruce trees in the eastern Canadian taiga  
835 Dendrochronologia 64:125771 doi:<https://doi.org/10.1016/j.dendro.2020.125771>

836 Wigley TML, Briffa KR, Jones PD (1984) On the Average Value of Correlated Time Series, with  
837 Applications in Dendroclimatology and Hydrometeorology Journal of Climate and  
838 Applied Meteorology 23:201-213 doi:10.1175/1520-  
839 0450(1984)023<0201:otavoc>2.0.co;2

840 Wilkinson S, Ogée J, Domec J-C, Rayment M, Wingate L (2015) Biophysical modelling of intra-  
841 ring variations in tracheid features and wood density of *Pinus pinaster* trees exposed  
842 to seasonal droughts Tree physiology 35:305-318 doi:10.1093/treephys/tpv010

843 Wilson R et al. (2021) Evaluating the dendroclimatological potential of blue intensity on  
844 multiple conifer species from Australasia Biogeosciences Discuss 2021:1-41  
845 doi:10.5194/bg-2021-119

846 Wilson R et al. (2019) Improved dendroclimatic calibration using blue intensity in the southern  
847 Yukon The Holocene 29:1817-1830 doi:10.1177/0959683619862037

848 Wilson R et al. (2016) Last millennium northern hemisphere summer temperatures from tree  
849 rings: Part I: The long term context *Quaternary Science Reviews* 134:1-18  
850 doi:<https://doi.org/10.1016/j.quascirev.2015.12.005>  
851 Wilson R, Rao R, Rydval M, Wood C, Larsson L-Å, Luckman BH (2014) Blue Intensity for  
852 dendroclimatology: The BC blues: A case study from British Columbia, Canada *The*  
853 *Holocene* 24:1428-1438 doi:10.1177/0959683614544051  
854 Wilson RJS, Luckman BH (2003) Dendroclimatic reconstruction of maximum summer  
855 temperatures from upper treeline sites in Interior British Columbia, Canada *The*  
856 *Holocene* 13:851-861 doi:10.1191/0959683603hl663rp  
857 Zhang X, Vincent LA, Hogg W, Niitsoo A (2000) Temperature and precipitation trends in  
858 Canada during the 20th century *Atmosphere-ocean* 38:395-429  
859 Ziaco E (2020) A phenology-based approach to the analysis of conifers intra-annual xylem  
860 anatomy in water-limited environments *Dendrochronologia* 59:125662  
861 doi:<https://doi.org/10.1016/j.dendro.2019.125662>  
862